

Speech2Lip: High-fidelity Speech to Lip Generation by Learning from a Short Video

Xiuzhe Wu¹, Pengfei Hu², Yang Wu^{3,4}, Xiaoyang Lyu¹, Yan-Pei Cao³, Ying Shan³, Wenming Yang², Zhongqian Sun⁴, Xiaojuan Qi¹,

¹The University of Hong Kong, ² Tsinghua University, ³ ARC Lab, Tencent PCG, ⁴ Tencent AI Lab

Abstract

Synthesizing realistic videos according to a given speech is still an open challenge. Previous works have been plagued by issues such as inaccurate lip shape generation and poor image quality. The key reason is that only motions and appearances on limited facial areas (e.g., lip area) are mainly driven by the input speech. Therefore, directly learning a mapping function from speech to the entire head image is prone to ambiguity, particularly when using a short video for training. We thus propose a decomposition-synthesis-composition framework named *Speech to Lip (Speech2Lip)* that disentangles speech-sensitive and speech-insensitive motion/appearance to facilitate effective learning from limited training data, resulting in the generation of natural-looking videos. First, given a fixed head pose (i.e., canonical space), we present a speech-driven implicit model for lip image generation which concentrates on learning speech-sensitive motion and appearance. Next, to model the major speech-insensitive motion (i.e., head movement), we introduce a geometry-aware mutual explicit mapping (GEMEM) module that establishes geometric mappings between different head poses. This allows us to paste generated lip images at the canonical space onto head images with arbitrary poses and synthesize talking videos with natural head movements. In addition, a Blend-Net and a contrastive sync loss are introduced to enhance the overall synthesis performance. Quantitative and qualitative results on three benchmarks demonstrate that our model can be trained by a video of just a few minutes in length and achieve state-of-the-art performance in both visual quality and speech-visual synchronization. Code: <https://github.com/CVMI-Lab/Speech2Lip>.

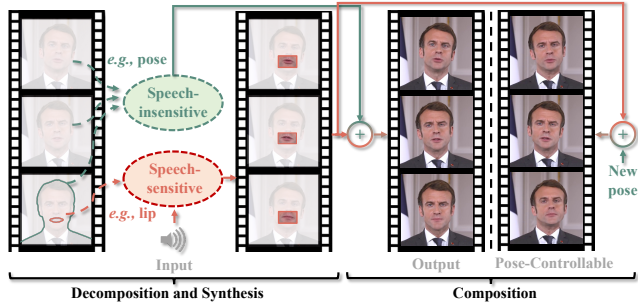


Figure 1. Given a speech as input, our model generates high-quality talking-head videos and supports pose-controllable synthesis. The decomposition and synthesis modules make learning from a short video more effective and the composition module enables us to synthesize high-fidelity videos.

1. Introduction

Learning from a short video to generate personalized audio-synchronized talking videos driven by a speech is of great importance to various applications, for instance, digital human animation, video dubbing, and UGC video creation. However, synthesizing high-fidelity videos from speech for a desired speaker remains a challenging task.

The first challenge arises from *complicated motion patterns*. Although speech majorly influences lip areas (i.e., speech-sensitive areas), lip movements are often accompanied by other motions, such as global head movements, which greatly impact lip shapes and appearances. Thus, directly synthesizing a whole image from speech often leads to inaccurate lip synthesis. Second, existing methods still struggle to satisfy *appearance fidelity* requirements, which include both identity preservation (speaker-specific) and high-quality detail generation, such as clear details of teeth, tongue, and eye-blinking [9, 42, 26, 44, 7]. Third, it’s difficult to *acquire videos longer than 10 hours* for a speaker which is yet required by conventional methods [17, 31].

To tackle the aforementioned challenges, existing attempts can be coarsely categorized into two lines of research: speaker-independent and speaker-specific methods. The first line often exploits GANs [15] that need to be trained on large-scale multi-person datasets. However, GAN-based models [4, 7, 9, 26, 33, 38, 42, 43] usually synthesize low-resolution images and unnatural motions (*i.e.*, background movements). They thus hardly meet the appearance fidelity requirement in terms of sharpness and fine appearance details. Moreover, preserving the identity of the speaker remains a challenging task [7, 43].

For the consideration of high-fidelity and identity preservation, another strategy focuses on learning from a specific speaker. Although attaining high-fidelity results, early works [17, 31] often require several hours of video footage from a speaker for training, hindering their practical applicability. Recently, NeRF [20] has emerged as a promising approach for generating high-fidelity videos, which succeeds in learning from a short video of just a few minutes and having the potential to generate high-fidelity results [16, 18, 28]. Nevertheless, the models still struggle with appearance and motion ambiguity issues because they model speech-sensitive motions/appearances together with other facial areas less correlated to the given speech. This issue becomes more severe when training data is limited since no extra information can be exploited to avoid interference from signals that are not correlated with the speech. As a result, they tend to generate lip sequences that do not synchronize well with the speech and produce blurry images (see Figure 5 and Table 1). Therefore, reducing the complexity of modeling motions is critical to enable effective learning from a short video and synthesizing high-quality videos for a specific speaker.

We thus design a preliminary experiment to identify that motion and appearance of lip areas have a strong correlation with speech, while head motion and other facial areas are less related to speech. Motivated by the observation, we propose decomposing speech-insensitive motion/appearance from speech-sensitive one, and synthesizing them separately before composing them into a new talking video that aligns with the given speech (Figure 1). Toward this goal, we present a decomposition-synthesis-composition framework named **Speech to Lip (Speech2Lip)**. In the decomposition stage, we introduce a speech-driven implicit model that generates high-fidelity synced lip sequences in a fixed view (*i.e.*, canonical view). To model 3D head motion effectively, we design a Geometry-Aware Mutual Explicit Mapping (GAMEM) module that estimates explicit geometric mappings between an arbitrary observed view and the canonical view. GAMEM also includes a jointly optimized canonical-view full-head depth map, which enables the model to be 3D-aware and supports controllable synthesis driven by new

head poses. In the composition stage, GAMEM allows us to flexibly paste the synthesized canonical-view lips onto an arbitrary observed view to obtain natural synchronized talking videos. To improve the synthesis and synchronization qualities after composition, we incorporate a blending network (*i.e.*, Blend-Net) to refine the results and a contrastive sync loss to facilitate learning from a short video for generating synchronized talking videos.

Our major contributions are summarized as follows:

- 1) We introduce a novel framework that disentangles speech-sensitive and speech-insensitive motion/appearance in high-fidelity video synthesis. By separating these components, the framework can effectively learn from limited training data.
- 2) The proposed speech-driven implicit model synthesizes speech-sensitive contents and the GAMEM flexibly combines them with given speech-insensitive areas to generate synchronized talking heads with natural movements and support pose-controllable synthesis.
- 3) Both qualitative and quantitative experimental results demonstrate the superiority of our method over the state-of-the-art speaker-specific methods.

2. Related Work

Speech-Driven Talking Face Synthesis. Video synthesis from speech is a long-standing problem. Recent works can be generally divided into two categories: speaker-specific [17, 31, 19, 16, 39, 18, 28] and speaker-independent [9, 42, 26, 44, 7, 5, 41, 35, 36]. In the first track, earlier works have succeeded in obtaining realistic visual results for a target person [17, 31] but required hours of video belonging to one specific speaker. Therefore, many efforts [19, 16, 39, 18, 28] have been made to train the model with a shorter talking video (3-5 minutes). However, they utilize speech to forecast overall motions including speech-insensitive ones, failing to learn accurate lip shapes and appearances. The other line (*i.e.*, speaker-independent method) aims to build a universal model for all identities [9, 42, 26, 44, 7]. The end-to-end pipeline [9, 42] is usually developed on GAN [15]. To boost performance, Richard *et al.* [27] only synthesize the mesh of limited facial areas, Prajwal *et al.* [26] present an extra lip-sync discriminator, Zhou *et al.* [43] provide additional head poses as inputs, and some other models [7, 14, 44, 32, 30] leverage the intermediate representation (*e.g.*, 2D facial landmarks [7, 14, 44] or expression parameters [32, 30]). Nevertheless, they often suffer from low video quality, difficult identity preservation, and abnormal head motion generation.

Implicit Representation based Talking Head Methods. Recently, implicit representations have shown high model-

ing capabilities in multiple tasks [25, 20, 24, 34]. Among them, NeRF [20] obtains extraordinary performance in novel view synthesis by training on only hundreds of images. Guo *et al.* [16] first apply it in the speaker-specific talking head synthesis task to enable learning from a short video. However, they utilize two NeRFs to model the head and torso, resulting in the head-torso separation phenomenon. Liu *et al.* [18] solve it by leveraging one unified NeRF with two semantic-aware modules. Shen *et al.* [28] incorporate 2D image features as additional inputs to further reduce training data requirements (*i.e.*, videos with only 10-15 seconds). Regardless, these methods only ensure visual quality, and simply use speech to drive all the complex motions, leading to the out-of-sync problem.

3. Empirical Study and Motivations

Our approach is motivated by the observation that only limited facial areas are highly correlated to speech. To verify this, we conduct a preliminary experiment to determine which areas are most speech-sensitive. Specifically, we apply warping to all captured images with varying head poses (refer to observed views) using the 3D Morphable Model (3DMM) [2] and bring them to a fixed head pose (known as the canonical view). We then compute a motion heatmap in the canonical view to determine the areas most responsive to speech. As depicted in Figure 2, the elimination of head motion results in most of the motions around the lip regions displaying high sensitivity to the input speech. Additional examples can be found in the supplementary file. For more details on the warping process, please refer to Sec. 4.3.

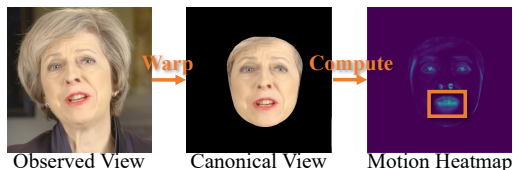


Figure 2. Speech-sensitive Motion Heatmap.

4. Method

4.1. Overview

Figure 3 provides an overview of our model. We define each frame captured in the observed view with its own head motion as the “observed space”. To disentangle speech-sensitive and speech-insensitive motions (*i.e.*, head motions), we randomly select one observed space to serve as the “canonical space”. By doing so, we are able to align all observed spaces with the canonical space, thereby eliminating the effects of head motions. Note that once selected, the canonical space is fixed during training and inference. To model speech-sensitive motions, we propose a speech-driven implicit model to generate lip images in the canonical space without head motion effect (Sec. 4.2). Thus, the generated lip image is canonical-view. A Geometry-Aware

Mutual Explicit Mapping (GAMEM) module is further proposed to model the speech-insensitive head motions without speech effect. Next, we project the lip images in canonical space generated by the above implicit model to the observed space based on GAMEM so that the synthesized lip image can be aligned and composed with any arbitrary observed frame, giving the model the flexibility for diversified composition (Sec. 4.3). Finally, a blending network (*i.e.*, BlendNet) and a contrastive sync loss are presented to improve the quality of final synthetic images \hat{I}_o (Sec. 4.4).

4.2. Disentangled and Synced Implicit Modeling

The central part of Speech2Lip is the disentangled and synced speech-driven implicit generator (Figure 3(a)), which focuses on generating 2D lip appearances that are synchronized with cross-modal speech. By employing motion and appearance disentanglement, the generator only retains speech-sensitive motions and appearances. A lip-syncing contrastive loss is utilized (Figure 3(c)) so that it can generate synced high-fidelity mouth appearance by learning from very short video data. All these together make the implicit modeling disentangled and synced.

Speech-driven Implicit Model To achieve high-fidelity canonical lip image generation, we utilize a speech-driven implicit model. An implicit model is defined as a function that maps the coordinate signal to another signal [29], *e.g.*, color. The input coordinates of the implicit model are defined in a continuous space (*i.e.*, the real field) so that it helps exploit the inherent relationship between spatially adjacent locations. Also, it can be further mapped into the frequency domain and benefit the learning of high-frequency information [20]. Besides, by learning a dedicated model for a specific scenario, implicit models also gain a strong ability to generate high-quality desired outputs. In our model, color information $\hat{c}_{c,n} = (r, g, b)$ is regarded as our output signal (appearance color), and the canonical implicit function f_θ can be defined as

$$\hat{c}_{c,n} = f_\theta(x_{c,n}, \mathbf{a}, t_s), \quad (1)$$

where $x_{c,n}$ is the continuous 2D pixel coordinate vector (u,v) in the canonical space. $\mathbf{a} \in \mathbb{R}^{64}$ is the feature vector of the input speech at the concerned moment and t_s represents the timestamp information, which is utilized to enhance the temporal consistency between adjacent frames.

Continuous Sampling The next question that arises is how to obtain the corresponding supervision signal to train the implicit model, which poses a challenge as the coordinates of the pixels are always integers, while we define the coordinates in a continuous space for more expressive features. To overcome this challenge, we adopt the approach developed in [8], which enables us to sample and generate corresponding supervisions in the continuous coordinate space.

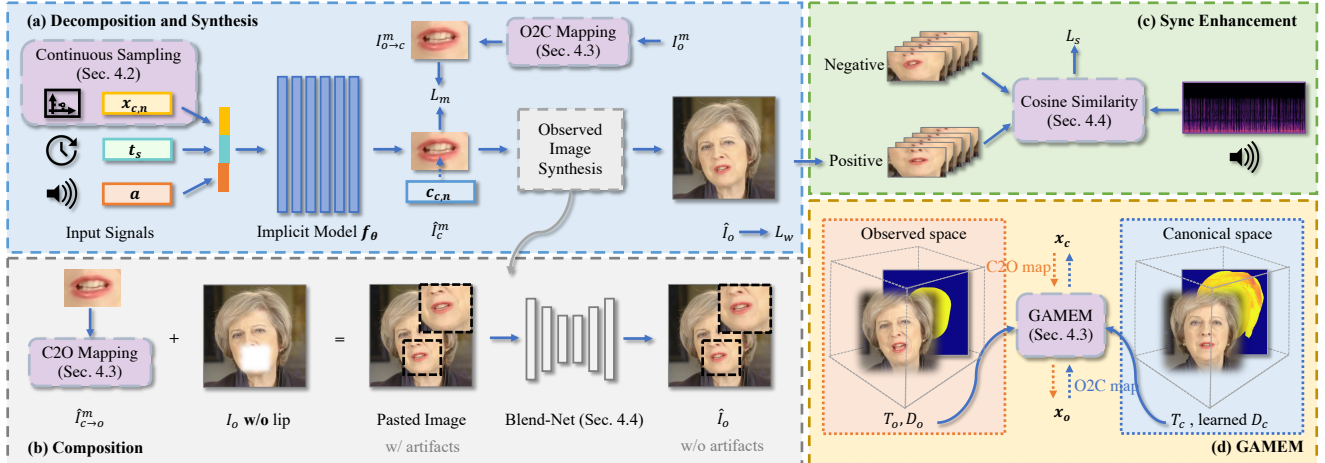


Figure 3. The overall framework of Speech2Lip. Our framework decomposes speech-sensitive and speech-insensitive motions/appearances first, models them individually (the major part of (a)), and composes the ultimate output image (b). Besides, the synchronization performance enhancement module and the GAMEM are illustrated in (c) and (d), respectively. The inputs include continuous pixel coordinates, speech audio signals, and timestamps. The speech-driven implicit model will generate speech-sensitive canonical-view lip images, which will be further transformed into observed space to compose the eventual output image. A full-head depth map is learned along with the training process, supporting pose-controllable synthesis.

Particularly, for each pixel x_c , a rectangle with an arbitrary shape is randomly sampled, the four corner points (*i.e.*, $x_{c,n}$, $n \in \{00, 01, 10, 11\}$) of which are regarded as our inputs. A weighted averaged value \hat{c}_c is then calculated as

$$\hat{c}_c = \sum_{n \in \{00, 01, 10, 11\}} \frac{S_n}{S} \cdot \hat{c}_{c,n}, \quad (2)$$

where $\hat{c}_{c,n}$ are the output appearance values of the sampled points. As illustrated in Figure 4, the blue-dashed-line rectangle represents the area S , which is divided into four sub-rectangles by gray lines, each with an area S_n . By leveraging this strategy, we can generate supervision for points with continuous positions, which enables us to fully exploit the advantages of the implicit model and achieve high-fidelity visual results.

4.3. Geometry-Aware Mutual Explicit Mapping

Once we have obtained the speech-sensitive lip sequences in the canonical view, we can construct the eventually synthesized image \hat{I}_o by assigning the synthesized pixels to a location in the observed space. However, since the assigning process is speech-insensitive and only relies on the geometry information, we introduce the GAMEM module, illustrated in Figure 3, to explicitly model it. The GAMEM module comprises Canonical-to-Observed (C2O), Observed-to-Canonical (O2C) Mapping, and a learnable full-head depth map, which supports various applications, including pose-controllable image synthesis.

C2O/O2C Mapping These mappings represent how the images transform between two spaces (*i.e.*, canonical space

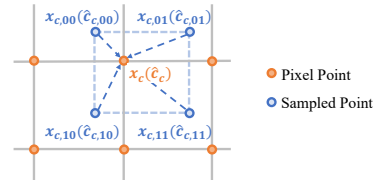


Figure 4. Continuous Sampling strategy. This strategy can generate supervision signals for sampled positions at different resolutions in the training time.

and observed space). As depicted in Figure 3, O2C Mapping aims at creating supervisions $I_{o \rightarrow c}^m$ for training the lip generator model f_θ and C2O Mapping is utilized to warp the generated lip image into the observed view to produce $\hat{I}_{c \rightarrow o}^m$ for further composition. As they follow similar principles, we take the O2C Mapping as an example to illustrate the process. The input of O2C Mapping contains I_o and I_c , and the output are pixel correspondences that map pixel coordinates in observed space to the canonical space. To achieve it, we use the 3D Morphable Model (3DMM) [2] to calculate the overall camera intrinsic matrix K and rough face geometry G . The head poses $T_o \in \mathbb{R}^{4 \times 4}$ and $T_c \in \mathbb{R}^{4 \times 4}$, which include a rotation matrix and a translation vector, are also estimated. And the relative head pose $T_{c \rightarrow o} \in \mathbb{R}^{4 \times 4}$ between two spaces can be computed as

$$T_{c \rightarrow o} = T_o \times T_c^{-1}. \quad (3)$$

Furthermore, *face* depth maps D_o and D_c for I_o and I_c obtained from 3DMM can be further interpolated based on G , and the corresponding head poses. Noticing that 3DMM can only be aware of the face area instead of the head area,

but the information about the rest part of the head (*e.g.*, forehead, ears, eyes, mouth) is lacking. Hence we optimize the D_c along with our model to complete the missing depth region. If p_o and p_c are the corresponding 2D homogeneous pixel grid coordinates on I_o and I_c , the geometric relationships can be explicitly formulated as

$$D_o p_o = K T_{c \rightarrow o} D_c K^{-1} p_c, \quad (4)$$

so the position mapping from canonical space to observed space can be easily obtained as

$$F_{c \rightarrow o}(T_{c \rightarrow o}, D_c, p_c) = p_o. \quad (5)$$

Then, we can warp the observed ground-truth lip images I_o^m into the canonical space by *backward warping*, denoted by $I_{o \rightarrow c}^m$, to guide the learning of the lip generation model. The C2O Mapping can be similarly defined by $T_{o \rightarrow c}$ and D_o . With it, we can warp the generated canonical lip image \hat{I}_c^m into the observed space by *backward warping*, denoted by $\hat{I}_{c \rightarrow o}^m$, to compose with the given observed image I_o for synthesizing a talking face.

Pose Controllable Synthesis Thanks to the simultaneously learned complete depth map D_c , pose-controllable full-head image synthesis according to users' requirements is also supported in our model. Specifically, we employ D_c to determine location correspondences based on Eq. 3 and Eq. 5 by altering T_o . There is a slight difference in this situation, which is to use the *forward warping* strategy as the ground-truth depths at new given poses are missing, which will produce black holes. To mitigate this issue, we propose a data augmentation method in training by randomly adding black holes with a ratio of 50% to the image to let the Blend-Net learn to fill these areas.

4.4. Overall Refinement

Image Blending With $\hat{I}_{c \rightarrow o}^m$, we can integrate it by directly pasting it to the original observed frame based on 2D lip landmarks [3]. However, the paste operation often results in mismatching artifacts in the boundary area, and the image artifacts after data augmentation should also be modified. Therefore, we propose a Blend-Net for blending. The Blend-Net takes the pasted image after the paste operation as input to synthesize harmonized final output \hat{I}_o . Since the target is fusion and amending instead of generation, we predict the pixel residual, which is further added back to the input image to composite the final output image. Detailed network structure is illustrated in the supplementary file.

Synchronization Enhancement. To further improve the synchronization performance, we introduce a pre-trained sync expert network to boost the model's performance in synchronization inspiring by [26]. The sync expert network consists of two pre-trained encoders, which extract features

of image and speech audio within a sliding window, denoted by i and a respectively. Different from [26], we only have a short video for training. Therefore, the unsynced speech-image pairs are also exploited to construct the contrastive loss which helps avoid falling into a trivial solution. Its effectiveness is also verified in our experiments. The distance of synced speech-image pairs is desired to be closer while that of the unsynced speech-image pairs should be farther. Thus, we define a contrastive sync loss \mathcal{L}_s based on the metric which is widely used in contrastive learning:

$$\mathcal{L}_s = y \cdot (1 - \cos(i, a)) + (1 - y) \cdot \max(0, \cos(i, a)), \quad (6)$$

where \cos is the cosine similarity metric. $y = 1$ and $y = 0$ represent positive and negative speech-image pairs, respectively. For the input speech, the positive images are the matched images at the same timestamp while the negative images are randomly chosen at some timestamps else.

4.5. Training Objectives

Our whole pipeline is trained in a self-supervised manner using the observed frames to provide the supervisory signals. The overall loss includes a canonical mouth image reconstruction loss \mathcal{L}_m , a depth loss \mathcal{L}_d , a sync loss \mathcal{L}_s , and a whole observed image reconstruction loss \mathcal{L}_w .

\mathcal{L}_m measures the reconstruction error between the predicted lip image \hat{I}_c^m and ground-truth lip image $I_{o \rightarrow c}^m$ as

$$\mathcal{L}_m = \mathcal{L}_p(\hat{I}_c^m, I_{o \rightarrow c}^m) + \|\hat{I}_c^m - I_{o \rightarrow c}^m\|_2, \quad (7)$$

where $I_{o \rightarrow c}^m$ is the warped ground truth lip image using O2C space mapping (see the supplementary file for more details) and the widely-used perceptual loss \mathcal{L}_p is defined in [40]. Similarly, overall reconstruction loss \mathcal{L}_w is computed as

$$\mathcal{L}_w = \mathcal{L}_p(\hat{I}_o, I_o) + \|\hat{I}_o - I_o\|_2. \quad (8)$$

The canonical head depth map is initialized by the incomplete depth map computed by 3DMM and is trained with the help of the photometric loss as

$$\mathcal{L}_d = \|\hat{I}_{o \rightarrow c} - I_c\|_2, \quad (9)$$

where $\hat{I}_{o \rightarrow c}$ is the warped predicted image. With the contrastive sync loss (Sec. 4.4), the overall loss function is

$$\mathcal{L} = \omega_m \cdot \mathcal{L}_m + \omega_w \cdot \mathcal{L}_w + \omega_d \cdot \mathcal{L}_d + \omega_s \cdot \mathcal{L}_s. \quad (10)$$

Implementation details are shown in the supplementary file.

5. Experiments

5.1. Datasets and metrics

Datasets. We evaluate our algorithm and other methods on three datasets belonging to three specific speakers (Testset I, Testset II and Testset III) as recent speaker-specific

Method	Trained with large extra data	Testset I					Testset II					Testset III
		PSNR \uparrow	SSIM \uparrow	CPBD \uparrow	LMD \downarrow	Sync \uparrow	PSNR \uparrow	SSIM \uparrow	CPBD \uparrow	LMD \downarrow	Sync \uparrow	Sync \uparrow
<i>Ground Truth</i>	<i>N/A</i>	<i>N/A</i>	<i>1.000</i>	<i>0.186</i>	<i>0.000</i>	<i>9.102</i>	<i>N/A</i>	<i>1.000</i>	<i>0.121</i>	<i>0.000</i>	<i>8.688</i>	<i>4.877</i>
ATVG [7]	Yes	28.452	0.818	0.019	5.423	5.813	28.051	0.668	0.003	4.203	6.224	3.571
MakeitTalk [44]	Yes	29.692	0.906	0.050	4.215	4.115	28.996	0.813	0.061	4.463	5.559	2.320
Wav2Lip [26]	Yes	31.557	0.980	0.115	3.053	10.031	31.793	0.956	0.065	3.415	9.936	5.809
PC-AVS [43]	Yes	29.072	0.880	0.040	4.595	9.258	28.359	0.734	0.046	4.305	8.586	5.206
LSP [19]	No	29.515	0.900	0.098	3.174	5.377	28.895	0.776	0.117	4.972	6.811	3.046
AD-NeRF [16]	No	32.223	0.954	0.051	2.989	6.042	30.885	0.909	0.055	3.210	5.910	3.285
DFRF [28]	No	33.292	0.974	0.094	3.079	5.252	31.419	0.944	0.124	3.139	5.552	2.879
Speech2Lip	No	34.815	0.987	0.224	2.976	7.771	33.197	0.962	0.125	3.082	7.370	4.379

Table 1. Quantitative results compared with the SOTA methods. Image quality assessment metrics (*i.e.*, PSNR, SSIM, and CPBD) are computed within **mouth region**. Algorithms are categorized into two classes based on the training datasets for a fair comparison. The first ones are trained in large public datasets while the other ones are trained using only 3-5min videos. The best results of each class are in **bold** and overall best results are with underlines.

methods [16, 19] usually do. Training videos are collected from [19] as they are publicly available. All video sequences are resampled to 25 FPS and split into training part and test part with a ratio of 90%/10%. The training splits of Testset I (500×500) and Testset II (624×624) are employed to train the models and then same-identity evaluations are conducted on the test splits. Testset III is utilized for cross-identity, -gender, and -language tests. We present more evaluation results in the supplementary file.

Evaluation Metrics. Since both face generation and lip generation models are contained in our quantitative evaluations, we conduct the image quality assessment just around the **mouth region** for a fair comparison. To evaluate the appearance quality, we first utilize image quality metrics Peak Signal-to-Noise Ratio (PSNR) and SSIM [37]. A no-reference objective image sharpness metric based on Cumulative Probability of Blur Detection (CPBD) [23, 21, 22] is further utilized to measure the overall perceptual image quality. For synchronization evaluation, Landmarks Distance (LMD) around the **mouth region** is exploited to compute the accuracy of lip shape following [6]. The confidence score of lip synchronization computed by a pre-trained SyncNet [12] is also applied to measure the synchronization performance, labeled by Sync.

5.2. Comparisons with State of the Arts

Same-identity Evaluation. For speaker-independent models, we conduct experiments using their officially released pre-trained models. Since AD-NeRF [16] and DFRF [28] are speaker-specific models, we retrain them using our training data for a fair comparison. DFRF aims at few-shot learning but its lip synchronization performance witnesses a significant drop when the number of training images decreases from 5000 to 15. Hence, we still train DFRF on thousands of images. Also, we directly use LSP’s [19] pre-trained models on Testset I and Testset II to conduct experi-

ments (subject May for Testset I and Testset III, and subject Obama2 for Testset II). We cannot provide a quantitative comparison with SSP-NeRF [18] here, as neither codes nor pre-trained weights are available. Thus, for comparison, we extract the speech from their released demo and then present qualitative comparisons in the supplementary file.

Quantitative results are shown in Table 1. We divide all the models into two types based on the scale of the training dataset. The upper four algorithms (speaker-independent models) are trained using public video datasets with large amounts of identities and speech-image pairs (*e.g.*, LRS2 [1, 11, 13] and VoxCeleb2 [10]) while the latter four methods (speaker-specific models) only use 5-minute videos of a specific identity for training. Speaker-independent models tend to perform well in synchronization because they can learn lip motions well from various speech-visual pairs in training time. However, the cost is sacrificing the visual quality. The metrics of image quality (*e.g.*, PSNR, SSIM, and CPBD) are much lower than that of specific models. Wav2lip [26] is an exception because it only generates lip images, but the details still can not be produced well (Figure 5). In contrast, speaker-specific models usually have much better image qualities, which is favorable in practice. Our model outperforms all the SOTA algorithms in image quality and achieves the best synchronization performance among all the speaker-specific models, and the Sync score is also competitive when compared to those speaker-independent models. It is also worth mentioning that the Sync scores of Wav2lip [26] and PC-AVS [43] are higher than that of the ground truth. The reason might be that the Sync score is sensitive to synchronization quality only when synchronization quality is within a range and a higher score above a threshold may not necessarily imply a higher synchronization quality. We design a toy experiment to verify it in the supplementary file and our user study can also demonstrate it.

Cross-identity Evaluation. Our model also has the abil-

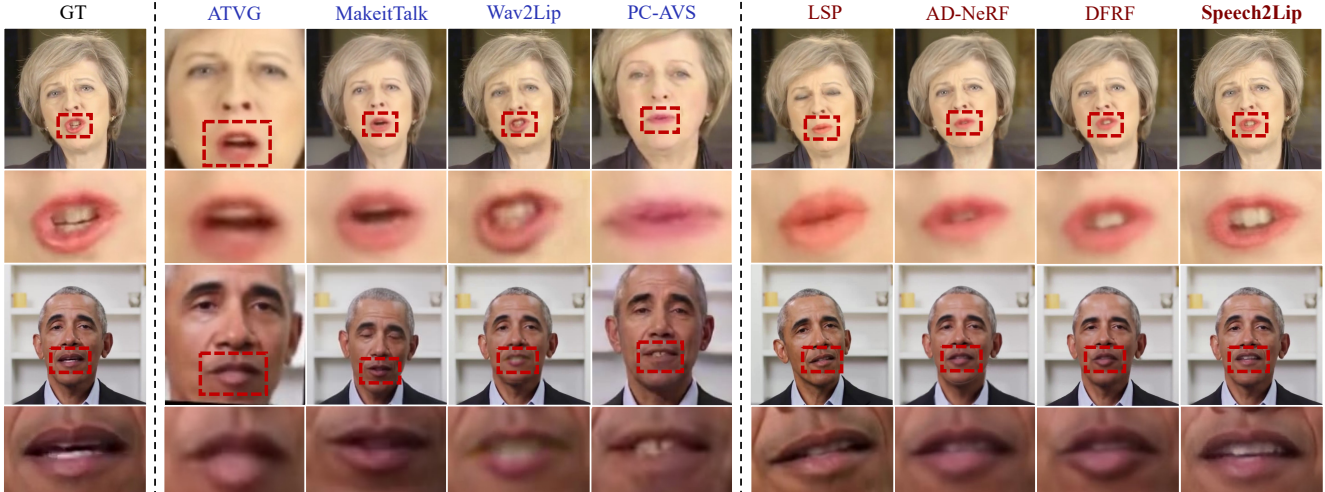


Figure 5. Qualitative results compared with SOTA methods. The Lip area is cropped based on the detected 2D landmarks for a clear comparison. **Speaker-independent** and **speaker-specific** models are remarked by different colors.

ity to generate cross-identity, -gender, and -language results. Since there is no ground truth image, we provide the sync performance comparison on generating a video for the model trained on Testset I (female, British) using another speaker’s speech (male, French). This setting is defined as Testset III, and results are shown in the last column of Table 1. Our model still has significant superiority and outperforms other speaker-specific models by a large margin. We also test the effect of unsynced speech-image pairs used in Eq. 6 on Testset III. Without negative pairs, the Sync score decreases from 4.379 to 3.830, showing the effectiveness of our contrastive sync loss.

Qualitative Results. Qualitative comparisons of different algorithms are presented in Figure 5. We can see that speaker-independent methods all suffer from low image quality. Besides, ATVG and MakeitTalk have unnatural speech-insensitive movements (*e.g.*, head motion and background motion) and PC-AVS has an extra issue of struggling with identity preservation. Speaker-specific approaches have much better visual quality but most of them can hardly estimate precise lip details when there exist considerable significant lip motions. And fine details like teeth and tongue are not well modeled either. Besides, AD-NeRF sometimes causes head-torso separation due to the adoption of two separate NeRFs. In contrast, our method Speech2Lip performs well in all these situations, as the generated shapes are more accurate and the synthetic images are clearer and more realistic especially the lip area. More results can be found in the supplementary videos.

Complexity Comparisons. To further demonstrate the superiority of our model, complexity and computational cost comparisons with speaker-specific models are conducted on Testset I. In Table 2, our model gains the best results with much less complexity and lower computational cost.

Methods	LSP	AD-NeRF	DFRF	Ours
Model size (MB) ↓	500	<u>30</u>	20	<u>30</u>
Train time (hour) ↓	<u>38.5</u>	80	60	30
Test speed (FPS) ↑	35	0.06	0.04	18
PSNR (dB) ↑	29.52	32.22	<u>33.29</u>	34.82
Sync ↑	5.38	<u>6.04</u>	5.25	7.77

Table 2. Speaker-specific model comparisons. The best results are in **bold** and the second best results are with underlines.

User Study. To verify the perceptual quality, user studies are conducted on 16 generated video clips covering both Testset I and Testset II. Videos are generated by our proposed Speech2Lip and other SOTA algorithms, with algorithm names hidden and video order randomized. 17 participants independently evaluated all the videos. For each video, each participant gave a Mean Opinion Score (MOS) from 1-5 for each of three aspects: qualities of speech-visual synchronization, image fidelity, and image realism. Higher scores represent better quality. The overall results are shown in Table 3. Speech2Lip not only achieves the highest MOS in image quality measurement (*e.g.*, 4.618 and 4.382) but also outperforms all the other algorithms in lip synchronization (*e.g.*, 4.265), exhibiting Speech2Lip has the most satisfactory overall video quality.

5.3. Ablation Study

Contributions of loss functions. We first conduct an ablation study on loss functions. The evaluation metrics contain the PSNR around the lip area and the sync score. The PSNR of the whole image is also retained since practical applications attach more attention to the overall quality of the talking portrait scene. Results are shown in Table 4, demonstrating the loss functions all contribute to the increased performance on both visual quality and synchronization.

Methods	ATVG	MakeitTalk	Wav2Lip	PC-AVS	LSP	AD-NeRF	DFRF	Speech2Lip
Lip Synchronization	1.500	1.853	4.191	3.059	3.118	3.088	2.853	4.265
Image Fidelity	1.147	2.794	3.265	2.529	3.882	3.235	3.265	4.618
Image Realness	1.118	2.088	3.765	2.265	3.000	2.324	2.971	4.382

Table 3. Detailed user study results compared with SOTA methods. The best results are in **bold**.

Methods	PSNR _{lip} ↑	PSNR _{img} ↑	Sync ↑
\mathcal{L}_w	34.104	36.947	6.313
$\mathcal{L}_w + \mathcal{L}_d$	34.429	36.994	6.359
$\mathcal{L}_w + \mathcal{L}_d + \mathcal{L}_m$	34.694	37.193	7.194
$\mathcal{L}_w + \mathcal{L}_d + \mathcal{L}_m + \mathcal{L}_s$	34.815	37.245	7.771

Table 4. Ablation study results about loss function on Testset I.

Methods	PSNR _{lip} ↑	PSNR _{img} ↑	Sync ↑
w/o continuous sampling	34.702	37.214	7.553
w/o implicit model	34.250	37.058	6.790
w/o Blend-Net	33.736	36.881	6.065
w/o time	34.512	37.121	7.146
Speech2Lip	34.815	37.245	7.771

Table 5. Ablation study results about network design on Testset I.

Contributions of individual components. We also explore the benefits of our key components by removing each component to see how the performance changes in Table 5. “**w/o** implicit model” represents we employ an explicit lip generation model instead, and “**w/o** time” indicates timestamp is deleted from inputs. From the results, it can be concluded that each design plays an important role. Among them, the Blend-Net significantly improves video quality, and the design of implicit modeling schema is also critical.

5.4. Controllable Synthesis Results

Thanks to the joint optimization and completion of a full-head depth map D_c in GAMEM, our model supports synthesizing full-head images driven by novel head poses. Specifically, D_c can be projected into any observed view to obtain D_o . D_c and T_o in Eq. (3) are further replaced by D_o and the new target head pose, respectively. Then, we adopt Eq. (5) to calculate the correspondence. The correspondence is further exploited to warp the synthesized image in the observed space into a new target space. It is noted that depth maps are used for coarse mapping between spaces while facial expression is more taken charge of by fine-grained contents from observed views. The pose-controllable novel view synthesis results are shown in Figure 7. When testing with moderate pose changes, our model achieves comparable results as AD-NeRF.

We note that existing methods with 3D modeling such as AD-NeRF also cannot generate good synthesis results if the evaluated poses deviate too much from the training data. The reason is that the training data widely used in speaker-specific models [19, 16, 28, 18] only show the front view

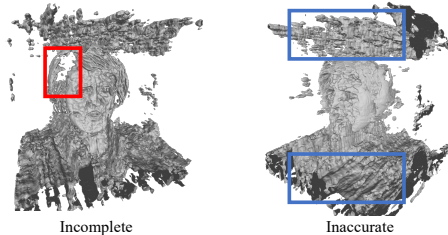


Figure 6. 3D Mesh of AD-NeRF on Testset I.



Figure 7. Novel view synthesis capability of our model. We rotate the head region with a random angle.

with limited pose variations, being naturally hard for 3D modeling. The 3D mesh is incomplete, and the surface is rough (Figure 6). In addition, the computational costs of 3D methods are extremely high (Table 2).

6. Conclusion

In this paper, we propose a novel decomposition-synthesis-composition framework called Speech2Lip for high-fidelity talking head video synthesis, which disentangles speech-sensitive and speech-insensitive motions/appearances. By presenting a synced speech-driven implicit model, a GAMEM module, a Blend-Net, and a contrastive sync loss, we can achieve satisfactory results with only a few minutes of training video. Our framework also supports pose-controllable synthesis. In the future, we plan to study generating realistic expressions driven by speech and explore combining our insights with advanced general image generation methods such as diffusion-based models for better generalizability. We hope that our work inspires more future research in this field and encourages the development of positive applications. However, we also urge caution to prevent any potential abuses. More discussions about limitations are described in the supplementary file.

Acknowledgement This work has been supported by the Research Fund from Tencent ARC lab.

References

- [1] T. Afouras, J. S. Chung, A. Senior, O. Vinyals, and A. Zisserman. Deep audio-visual speech recognition. In *arXiv:1809.02108*, 2018. 6
- [2] Volker Blanz and Thomas Vetter. A morphable model for the synthesis of 3d faces. In *Proceedings of the 26th annual conference on Computer graphics and interactive techniques*, pages 187–194, 1999. 3, 4
- [3] Adrian Bulat and Georgios Tzimiropoulos. How far are we from solving the 2d & 3d face alignment problem? (and a dataset of 230,000 3d facial landmarks). In *International Conference on Computer Vision*, 2017. 5
- [4] Lele Chen, Guofeng Cui, Ziyi Kou, Haitian Zheng, and Chenliang Xu. What comprises a good talking-head video generation? In *IEEE/CVF Conference on Computer Vision and Pattern Recognition Workshops*, 2020. 2
- [5] Lele Chen, Guofeng Cui, Celong Liu, Zhong Li, Ziyi Kou, Yi Xu, and Chenliang Xu. Talking-head generation with rhythmic head motion. In *Computer Vision—ECCV 2020: 16th European Conference, Glasgow, UK, August 23–28, 2020, Proceedings, Part IX*, pages 35–51. Springer, 2020. 2
- [6] Lele Chen, Zhiheng Li, Ross K Maddox, Zhiyao Duan, and Chenliang Xu. Lip movements generation at a glance. In *Proceedings of the European Conference on Computer Vision (ECCV)*, pages 520–535, 2018. 6
- [7] Lele Chen, Ross K Maddox, Zhiyao Duan, and Chenliang Xu. Hierarchical cross-modal talking face generation with dynamic pixel-wise loss. In *Proceedings of the IEEE/CVF Conference on Computer Vision and Pattern Recognition*, pages 7832–7841, 2019. 1, 2, 6
- [8] Yinbo Chen, Sifei Liu, and Xiaolong Wang. Learning continuous image representation with local implicit image function. In *Proceedings of the IEEE/CVF Conference on Computer Vision and Pattern Recognition*, pages 8628–8638, 2021. 3
- [9] Joon Son Chung, Amir Jamaludin, and Andrew Zisserman. You said that? *arXiv preprint arXiv:1705.02966*, 2017. 1, 2
- [10] Joon Son Chung, Arsha Nagrani, and Andrew Zisserman. Voxceleb2: Deep speaker recognition. *arXiv preprint arXiv:1806.05622*, 2018. 6
- [11] J. S. Chung, A. Senior, O. Vinyals, and A. Zisserman. Lip reading sentences in the wild. In *IEEE Conference on Computer Vision and Pattern Recognition*, 2017. 6
- [12] Joon Son Chung and Andrew Zisserman. Out of time: automated lip sync in the wild. In *Asian conference on computer vision*, pages 251–263. Springer, 2016. 6
- [13] J. S. Chung and A. Zisserman. Lip reading in profile. In *British Machine Vision Conference*, 2017. 6
- [14] Dipanjan Das, Sandika Biswas, Sanjana Sinha, and Brojeshwar Bhowmick. Speech-driven facial animation using cascaded gans for learning of motion and texture. In *European Conference on Computer Vision*, pages 408–424. Springer, 2020. 2
- [15] Ian Goodfellow, Jean Pouget-Abadie, Mehdi Mirza, Bing Xu, David Warde-Farley, Sherjil Ozair, Aaron Courville, and Yoshua Bengio. Generative adversarial nets. *Advances in neural information processing systems*, 27, 2014. 2
- [16] Yudong Guo, Keyu Chen, Sen Liang, Yong-Jin Liu, Hujun Bao, and Juyong Zhang. Ad-nerf: Audio driven neural radiance fields for talking head synthesis. In *Proceedings of the IEEE/CVF International Conference on Computer Vision*, pages 5784–5794, 2021. 2, 3, 6, 8
- [17] Rithesh Kumar, Jose Sotelo, Kundan Kumar, Alexandre de Brébisson, and Yoshua Bengio. Obamanet: Photo-realistic lip-sync from text. *arXiv preprint arXiv:1801.01442*, 2017. 1, 2
- [18] Xian Liu, Yinghao Xu, Qianyi Wu, Hang Zhou, Wayne Wu, and Bolei Zhou. Semantic-aware implicit neural audio-driven video portrait generation. *arXiv preprint arXiv:2201.07786*, 2022. 2, 3, 6, 8
- [19] Yuanxun Lu, Jinxiang Chai, and Xun Cao. Live speech portraits: real-time photorealistic talking-head animation. *ACM Transactions on Graphics (TOG)*, 40(6):1–17, 2021. 2, 6, 8
- [20] Ben Mildenhall, Pratul P Srinivasan, Matthew Tancik, Jonathan T Barron, Ravi Ramamoorthi, and Ren Ng. Nerf: Representing scenes as neural radiance fields for view synthesis. In *European conference on computer vision*, pages 405–421. Springer, 2020. 2, 3
- [21] Niranjan Narvekar and Lina J Karam. An improved no-reference sharpness metric based on the probability of blur detection. In *Workshop on Video Processing and Quality Metrics*, 2010. 6
- [22] Niranjan D Narvekar and Lina J Karam. A no-reference perceptual image sharpness metric based on a cumulative probability of blur detection. In *2009 International Workshop on Quality of Multimedia Experience*, pages 87–91. IEEE, 2009. 6
- [23] Niranjan D Narvekar and Lina J Karam. A no-reference image blur metric based on the cumulative probability of blur detection (cpbd). *IEEE Transactions on Image Processing*, 20(9):2678–2683, 2011. 6
- [24] Michael Oechsle, Songyou Peng, and Andreas Geiger. Unisurf: Unifying neural implicit surfaces and radiance fields for multi-view reconstruction. In *Proceedings of the IEEE/CVF International Conference on Computer Vision*, pages 5589–5599, 2021. 3
- [25] Jeong Joon Park, Peter Florence, Julian Straub, Richard Newcombe, and Steven Lovegrove. Deepsdf: Learning continuous signed distance functions for shape representation. In *Proceedings of the IEEE/CVF conference on computer vision and pattern recognition*, pages 165–174, 2019. 3
- [26] KR Prajwal, Rudrabha Mukhopadhyay, Vinay P Namboodiri, and CV Jawahar. A lip sync expert is all you need for speech to lip generation in the wild. In *Proceedings of the 28th ACM International Conference on Multimedia*, pages 484–492, 2020. 1, 2, 5, 6
- [27] Alexander Richard, Michael Zollhöfer, Yandong Wen, Fernando De la Torre, and Yaser Sheikh. Meshtalk: 3d face animation from speech using cross-modality disentanglement. In *Proceedings of the IEEE/CVF International Conference on Computer Vision*, pages 1173–1182, 2021. 2
- [28] Shuai Shen, Wanhua Li, Zheng Zhu, Yueqi Duan, Jie Zhou, and Jiwen Lu. Learning dynamic facial radiance fields for few-shot talking head synthesis. In *European conference on computer vision*, 2022. 2, 3, 6, 8

- [29] Vincent Sitzmann, Julien Martel, Alexander Bergman, David Lindell, and Gordon Wetzstein. Implicit neural representations with periodic activation functions. *Advances in Neural Information Processing Systems*, 33:7462–7473, 2020. 3
- [30] Linsen Song, Wayne Wu, Chen Qian, Ran He, and Chen Change Loy. Everybody’s talkin’: Let me talk as you want. *IEEE Transactions on Information Forensics and Security*, 2022. 2
- [31] Supasorn Suwajanakorn, Steven M Seitz, and Ira Kemelmacher-Shlizerman. Synthesizing obama: learning lip sync from audio. *ACM Transactions on Graphics (ToG)*, 36(4):1–13, 2017. 1, 2
- [32] Justus Thies, Mohamed Elgharib, Ayush Tewari, Christian Theobalt, and Matthias Nießner. Neural voice puppetry: Audio-driven facial reenactment. In *European conference on computer vision*, pages 716–731. Springer, 2020. 2
- [33] Konstantinos Vougioukas, Stavros Petridis, and Maja Pantic. Realistic speech-driven facial animation with gans. *International Journal of Computer Vision*, 128(5):1398–1413, 2020. 2
- [34] Peng Wang, Lingjie Liu, Yuan Liu, Christian Theobalt, Taku Komura, and Wenping Wang. Neus: Learning neural implicit surfaces by volume rendering for multi-view reconstruction. *arXiv preprint arXiv:2106.10689*, 2021. 3
- [35] Suzhen Wang, Lincheng Li, Yu Ding, Changjie Fan, and Xin Yu. Audio2head: Audio-driven one-shot talking-head generation with natural head motion. *arXiv preprint arXiv:2107.09293*, 2021. 2
- [36] Suzhen Wang, Lincheng Li, Yu Ding, and Xin Yu. One-shot talking face generation from single-speaker audio-visual correlation learning. In *Proceedings of the AAAI Conference on Artificial Intelligence*, volume 36, pages 2531–2539, 2022. 2
- [37] Zhou Wang, Alan C Bovik, Hamid R Sheikh, and Eero P Simoncelli. Image quality assessment: from error visibility to structural similarity. *IEEE transactions on image processing*, 13(4):600–612, 2004. 6
- [38] Olivia Wiles, A Koepke, and Andrew Zisserman. X2face: A network for controlling face generation using images, audio, and pose codes. In *Proceedings of the European conference on computer vision (ECCV)*, pages 670–686, 2018. 2
- [39] Shunyu Yao, RuiZhe Zhong, Yichao Yan, Guangtao Zhai, and Xiaokang Yang. Dfa-nerf: Personalized talking head generation via disentangled face attributes neural rendering. *arXiv preprint arXiv:2201.00791*, 2022. 2
- [40] Richard Zhang, Phillip Isola, Alexei A Efros, Eli Shechtman, and Oliver Wang. The unreasonable effectiveness of deep features as a perceptual metric. In *CVPR*, 2018. 5
- [41] Zhimeng Zhang, Lincheng Li, Yu Ding, and Changjie Fan. Flow-guided one-shot talking face generation with a high-resolution audio-visual dataset. In *Proceedings of the IEEE/CVF Conference on Computer Vision and Pattern Recognition*, pages 3661–3670, 2021. 2
- [42] Hang Zhou, Yu Liu, Ziwei Liu, Ping Luo, and Xiaogang Wang. Talking face generation by adversarially disentangled audio-visual representation. In *Proceedings of the AAAI conference on artificial intelligence*, volume 33, pages 9299–9306, 2019. 1, 2
- [43] Hang Zhou, Yasheng Sun, Wayne Wu, Chen Change Loy, Xiaogang Wang, and Ziwei Liu. Pose-controllable talking face generation by implicitly modularized audio-visual representation. In *Proceedings of the IEEE/CVF Conference on Computer Vision and Pattern Recognition*, pages 4176–4186, 2021. 2, 6
- [44] Yang Zhou, Xintong Han, Eli Shechtman, Jose Echevarria, Evangelos Kalogerakis, and Dingzeyu Li. Makelttalk: speaker-aware talking-head animation. *ACM Transactions on Graphics (TOG)*, 39(6):1–15, 2020. 1, 2, 6